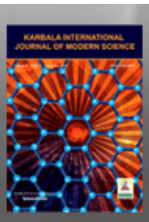

Karbala International Journal of Modern Science

Volume 6 | Issue 1 Article 14

Photo-physical properties of lanthanides doped O-bridged conducting indole oligomer

Iffat Ameen
D. D. U. Gorakhpur University, Gorakhpur, iffatameen@yahoo.in

Raj Laxmi Mishra
D. D. U. Gorakhpur University, Gorakhpur, raj.chem88@yahoo.com

Abhishek K. Tripathi
D. D. U. Gorakhpur University, Gorakhpur, abhigkp@yahoo.in

Afshan Siddiqui
D. D. U. Gorakhpur University, Gorakhpur, qaiser.gkp@gmail.com

Umesh N. Tripathi
Deen Dayal Upadhyay Gorakhpur University, Gorakhpur., un_tripathi@yahoo.com

Photo-physical properties of lanthanides doped O-bridged conducting indole oligomer

Abstract

The indole oligomers were synthesized by an effective green route in the water medium. This is an effort to synthesize commercially important indole oligomers without using any harmful chemicals and artificial media. The lanthanide chlorides such as $LaCl_3 \cdot 7H_2O$, $CeCl_3 \cdot 7H_2O$, $PrCl_3 \cdot 6H_2O$ and $NdCl_3 \cdot 6H_2O$ were used in the synthesis procedure to minimize the reaction time. Unlike the previous works, these reactions occurred at somewhat elevated temperature. In the reaction, the salts of lanthanide metals acted as a catalyst and further behave as dopants. These dopants increased the various properties (like conducting behavior) of the oligomers. The synthesized hetero-oligomers were characterized by different physicochemical and spectral techniques. The luminescence phenomenon was studied by the absorbance, excitation and emission peaks, justifying the upconversion phenomenon. The conducting behavior of these oligomers was studied at different concentrations to observe the dependence of the conduction of electrons at various concentrations. In this manuscript, we first time introduced the $LnCl_3 \cdot xH_2O$ to observe their behavior towards the reaction procedure, their doping behavior and the morphology of the synthesized oligomer particles. This study is an effort to synthesize the valuable indole oligomer via a more convenient way, which can be applicable in the field of luminescence, conductance, etc.

Keywords

Indole, hetero-oligomer, upconversion, green route, conducting behavior

Cover Page Footnote

The authors are grateful to SAIF, CDRI, Lucknow, India, SAIF, IIT Madras, India, STIC, Cochin, India and CECRI Karaikudi, India, for providing the necessary spectral and analytical data. We are also thankful to the Department of Chemistry, D. D. U. Gorakhpur University, Gorakhpur, India for providing the laboratory and library facilities.

1. Introduction

The conducting polymers have several applications in different fields like in diodes, capacitors, rechargeable batteries, LEDs, sensors, transistors, material science, agrochemical and biological areas [1−4]. The conducting polymer containing multiwall carbon nanotubes have the application in the adsorption and separation of cadmium and lead ions via solid-phase extraction, as the efficient sorbent for trace determination of cadmium and lead ions in water, in removal and trace detection of lead ions in food and environmental samples, as sorbent for solid-phase extraction of trace palladium ions in soil and water [5−8]. From the literature, it is also known that the PAN-based electrospun nanofiber webs containing Ni−ZnO can act as high-performance visible-light photocatalyst [9]. By perceiving the diverse application in the above fields and the demand of conducting polymers in bulk quantity, considerable attention has been devoted to the synthesis and study of these polymers. The indole is an organic species, having a benzene ring and a five-membered ring containing a heteroatom. Due to its structure indole itself has good electrical conductivity and thermal stability. To increase its various properties, the indole was polymerized by Taourillon and Garnier [10], by anodic oxidation. But the performance was not found satisfactory. After that, many efforts (like electrochemical oxidation, emulsion and interfacial polymerization, etc.) are made to synthesize more efficient polyindoles [11−14]. Most of the preparations involve the use of organic and harmful solvent media, artificial atmosphere, excess reaction time and eminent amount of oxidants. The resulting polymers are mostly insoluble, having applications like high redox activity and stability, slow degradation, used in anti-corrosion coatings, pharmacology, electrolysis, electrochemical cycling, drug delivery, etc. and show electrical conductivity in the range 10^{-1}-10^{-7} S/cm [11,12].

In the recent decade, some attention has been paid to controlling the particle morphology of polyindole [11]. The particles of these polymers are of different sizes and shapes and have promising applications in numerous areas [15−19]. There are several techniques to produce different sizes and shapes of polyindole particles [14,20−22]. For example; Katesara et al. used a surfactant to control the morphology of indole polymers [11].

After the thorough study of literature and by understanding the importance and demand, the polyindole was synthesized, characterized and applied to various aspects. There is a number of literatures are present in which dimers, trimers, and tetramers were synthesized [23,24]. Herein we report a pentamer of indoles, which are soluble in various organic solvents. Avoiding the use of harmful chemicals/solvents, here we outlined the eco-friendly and cost-effective methods of synthesis. To minimize the reaction time, to increase the conductance, to control the morphology and to study the unique upconversion (anti-Stokes type emission) phenomenon (in contrast to the previous reports), we introduced the salt of lanthanum, cerium, praseodymium, and neodymium in varying reaction media as doping agents and studied the effect of the addition of these salts. Since the conducting polymers also have applications in polymer solar cell, chemical sensors, chemiresistors, field-effect transistor (FET) sensors, corrosion protection etc. therefore having the indole unit and lanthanide element traces, these synthesized doped indole oligomers can also show these properties in great extent [25].

2. Methods of synthesis

All the reactions were carried out in an eco-friendly water environment. No any other solvents/acids/bases were used in these syntheses. Indole (Kemphasol, India), $LaCl_3 \cdot 7H_2O$ (S.D. Fine, India), $CeCl_3 \cdot 7H_2O$ (HPLC, India), $PrCl_3 \cdot 6H_2O$ (HPLC, India), and $NdCl_3 \cdot 6H_2O$ (HPLC, India), $FeCl_3$ (S.D. Fine, India) were used as purchased.

2.1. Synthesis of In−O−In

Indole and $FeCl_3$ were mixed in hot water in 4:1 M ratio. The content was stirred continuously for 16 h by increasing the temperature from 50 to 90 °C by a rate of 2.5 °C/h. After reducing the water, a soil colored precipitate was obtained, which was filtered by Whatman filter paper number 42 and washed thoroughly with cold and hot water. The details of synthesis are given in Table 1 and the reaction is given as Scheme 1.

https://doi.org/10.33640/2405-609X.1471

Table 1
Different reaction conditions for the polymerization of indole.

S. No.	Indole g (mmol)	$FeCl_3$ g (mmol)	$LnCl_3 \cdot xH_2O$ g (mmol)	Temp. (°C)	Reaction time (hours)	Color	% yield	Sample abbreviation
1	1 (8.53)	0.35 (2.13)	–	50−90	16	Soil	70	PIn
2	1 (8.53)	0.35 (2.13)	$LaCl_3 \cdot 7H_2O$ 0.79 (2.13)	50	3	Dark reddish-brown	89	La−PIn
3	1 (8.53)	0.35 (2.13)	$CeCl_3 \cdot 7H_2O$ 0.80 (2.13)	50	4	Dark brown	84	Ce−PIn
4	1 (8.53)	0.35 (2.13)	$PrCl_3 \cdot 6H_2O$ 0.76 (2.13)	50	4.5	Reddish-Brown	92	Pr−PIn
5	1 (8.53)	0.35 (2.13)	$NdCl_3 \cdot 6H_2O$ 0.76 (2.13)	50	5	Brown	80	Nd−PIn

2.2. Synthesis of In−O−In catalyzed by lanthanide metal salts

8.53 mmol of indole was dissolved in hot water (48 °C) and an aqueous of lanthanide metal salt was added to it. An aqueous solution of $FeCl_3$ was added in the above reaction mixture and stirred it for 3−5 h at 50 °C temperature. After reducing the water, some brown colored solid was obtained, which was filtered by Whatman filter paper number 42 and washed thoroughly with cold and hot water. Details of the reaction conditions are given in Table 1. The reaction proceeds in the process of the polymerization can be seen as Scheme 1.

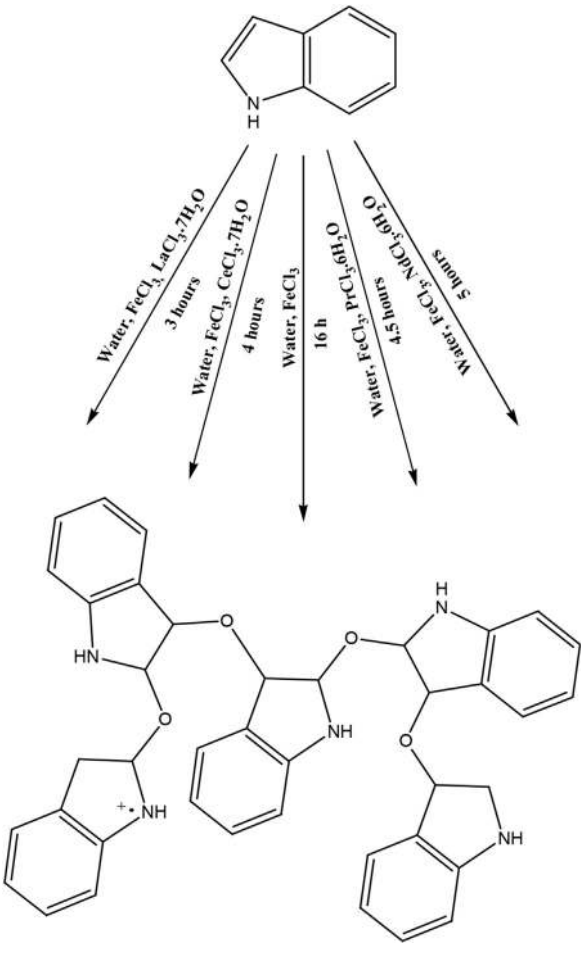

Scheme 1. Reaction pathways for synthesizing the indole oligomer.

3. Characterization techniques

FTIR spectral bands were obtained by a Thermo Nicolet spectrometer in the range 4000-400 cm^{-1} with the resolution 4 cm^{-1}. NMR bands were detected by Bruker Avance III FTNMR spectrometer, with frequency 400 MHz in DMSO solvent. Elemental analysis (C, H, and N) were carried out on an Elementar Vario EL III C, H, N, analyzer. Oxygen was analyzed by EuroVector elemental analyzer. To confirm the presence of the elements and the sizes of nanoparticles, SEM-EDX was carried out by F E I Quanta FEG 200−High-Resolution Scanning Electron Microscope. The TEM images were obtained by transmission electron microscope model Jeol 2100 at 200 kV using LaB_6 electron gun with point resolution 0.23 nm and lattice resolution 0.14 nm. Powder X-ray diffraction studies were carried out on model Bruker AXS D8 Advance diffractometer at temperature range −170 °C to +450 °C. The molecular ion peak was detected by Agilent 6520 Q-TOF (ESI-HRMS) spectrometer. The thermal behavior of the oligomers was studied by NETZSCH STA 449 F3 Jupiter thermal analyzer in a nitrogen atmosphere at 20 mL/min flow rate. The absorption, excitation and emission spectra were recorded in THF using Varian, Cary 5000 UV-visible spectrophotometer and Jobin Yvon Fluorolog-3-11 spectrofluorimeter. Electrical conductance was measured by Toshcon Auto Ranging Digital Conductivity/TDS Meter TCM 15+ in acetonitrile solution at different concentrations.

4. Results and discussion

All the oligomers synthesized by different techniques were different in color. The difference in color indicates the presence of different dopants in different materials. These all were stable in air and soluble in $CHCl_3$, ACN, THF, DCM solvents. Molecular weight measurement shows that these oligomers were pentameric in nature. The elemental analysis (C, H, N, and O) data are in accordance with the stoichiometry proposed. EDX and PXRD peaks indicate the presence of lanthanide elements in the materials. The analytical and physical details are given in Table 2.

4.1. FTIR spectral analysis

The FTIR studies of PIn have been well described in the literature [26]. The FTIR spectra of all the oligomers show the band in the range 3405–3413 cm^{-1} which confirms the presence of N–H bond [27,28] indicating the non-involvement of –NH group in the polymerization [29]. The stretching mode of the aromatic ring was indicated by the presence of bands in the range 1407–1623 cm^{-1} [30]. The C–N stretching band was found at 1331-1335 cm^{-1} [31]. The C–O–C bond was confirmed by the appearance of the band at 1095-1116 cm^{-1} [32,33]. Based on above, the 2nd and 3rd position of the five-membered ring is the point of polymerization [34,35]. The presence of the C–O–C bond peak indicates that the polymerization takes place by incorporation of oxygen moiety. The spectral bands are showing in Fig. 1, and details are given in Table 3.

4.2. FTNMR (^{1}H NMR) spectroscopic characterization

The characteristic signals in proton NMR of oligomers were detected by ^{1}H NMR spectra in deuterated dimethylsulfoxide (DMSO). The signal in the range δ 8.91–9.16 ppm, indicates the presence of N–H bond [36]. The presence of the N–H peak showing the non-involvement of –NH group which is also supported by FTIR spectra. The presence of aromatic protons was confirmed by the presence of multiplet in the range δ 7–8 ppm [37]. Peaks present at δ 7.23–7.25 and 6.54–6.56 ppm indicate the existence of the C–H bond of the 2nd and 3rd position of the five-membered ring [38]. A shifting in peaks in comparison to indole moiety shows the polymerization of indole moieties. The proton NMR spectral data for all of the oligomers have been summarized in Table 4 and the spectrum is given as Fig. 2.

4.3. ESI mass spectrometry

The molecular ion peaks were detected by the positive ESI method of mass spectrometry which confirms the molecular weight of the oligomers. The peak at m/z = 652.6963 (1), 652.6242 (2), 652.6711 (3), 652.6629 (4) and 652.7134 (5) ESI mass spectrum pattern confirms their existence as pentamers. The fragmentation patterns of these oligomers are also in support by the TGA-DTG decomposition pattern. The obtained molecular weights from the ESI pattern are given in Table 2.

4.4. EDX and PXRD studies

The EDX pattern shows the presence of elements in the synthesized indole oligomer. The peaks found in EDX are in good support of the elemental analysis done for the samples. The EDX images also indicate the presence of lanthanide elements in the indole oligomers. Since the percentage of these lanthanides is in very less quantity, therefore one can say that these elements can be present in the form of dopants. EDX images of all the synthesized oligomers are given as supplementary information SI 1 (a-d).

The presence of lanthanides can also be indicated by the PXRD peaks. Presence of peaks at $2\theta = 26.725°$

Table 2
Molecular weight and elemental analysis details.

S. No.	Oligomer	Mol. Wt. (m/z) Found (Calc.)	%C Obs (Calc.)	%H Obs (Calc.)	%N Obs (Calc.)	%O Obs (Calc.)
1	PIn	652.6963 (651.7513)	74.67 (74.71)	4.25 (4.24)	10.93 (10.91)	9.99 (9.97)
2	La–PIn	652.6242 (651.7513)	74.76 (74.71)	4.25 (4.24)	10.90 (10.91)	9.96 (9.97)
3	Ce–PIn	652.6711 (651.7513)	74.79 (74.71)	4.23 (4.24)	10.94 (10.91)	9.95 (9.97)
4	Pr–PIn	652.6629 (651.7513)	74.80 (74.71)	4.25 (4.24)	10.94 (10.91)	9.98 (9.97)
5	Nd–PIn	652.7134 (651.7513)	74.76 (74.71)	4.23 (4.24)	10.88 (10.91)	9.96 (9.97)

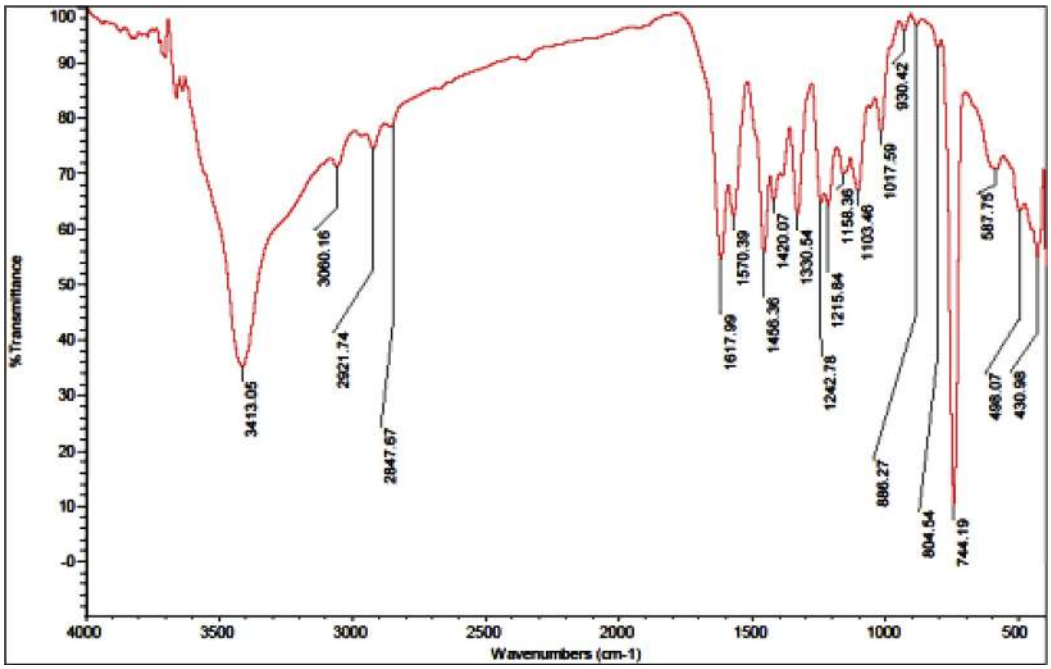

Fig. 1. FTIR spectral peaks of La−PIn.

Table 3
FTIR spectral peaks of oligomers.

S. No.	Oligomer	Wavenumbers ν (cm^{-1})				
		N−H	C−C stretching mode of aromatic ring	C−N stretching	C−O−C	C−H bending out of plane of benzene
1	PIn	3413	1420−1618	1331	1103	744
2	La−PIn	3405	1414−1617	1333	1095	741
3	Ce−PIn	3409	1411−1620	1332	1101	743
4	Pr−PIn	3412	1409−1623	1334	1116	742
5	Nd−PIn	3410	1407−1622	1335	1099	742

and 35.019° in the supplementary information (SI 2a) indicates the presence of lanthanum [39] whereas in case of praseodymium (SI 2b) these peaks are found at 2θ = 26.659°, 35.085° and 39.119° which shows the presence of praseodymium in indole oligomer [62]. The peaks at 2θ = 33.080° and 28.463° (SI 2c) in the sample Nd−PIn designate the existence of neodymium in these materials [40,41]. The appearance of peaks of La−PIn and Nd-PIn show the existence of these materials in microcrystalline form, whereas some sharp peaks of Pr−PIn indicate the crystalline nature of this material.

Table 4
Proton NMR shifts of oligomers.

S. No.	Oligomer	Chemical Shift δ (ppm)			
		N−H	C−H (Aromatic Ring)	C−H 2-Position	C−H 3-Position
1	PIn	8.91	7−8	7.24	6.56
2	La−PIn	9.01	7−8	7.23	6.54
3	Ce−PIn	9.16	7−8	7.23	6.55
4	Pr−PIn	9.11	7−8	7.24	6.54
5	Nd−PIn	9.14	7−8	7.25	6.56

The average crystallite size was calculated by the Debye-Scherer formula using the peaks having 2θ and FWHM value and these are given in Table 5. All these average crystallite size fall in the nanometer range.

4.5. TGA-DTG-DSC studies

The thermal behavior of the oligomers was studied by the TGA, DTG and DSC curves which were obtained by implying gradual heat from room temperature to 1400 °C in a nitrogen atmosphere. The TG-DSC curves can be seen in Fig. 3. All the differently synthesized oligomer of indole shows good resistivity

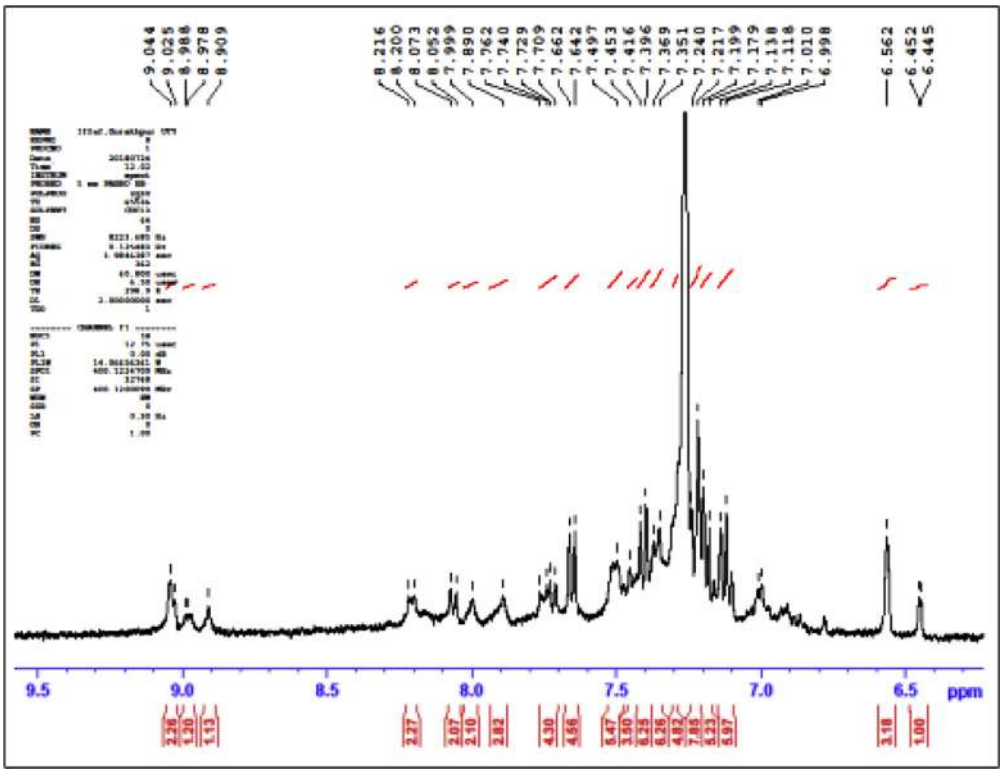

Fig. 2. ^{1}H NMR peaks of La–PIn.

Table 5
PXRD details of oligomers.

S. No.	Oligomer	2θ (°)	FWHM (mm)	Average crystallite size (nm)	Nature
1	La–PIn	08.280	3.83	47.37	Microcrystalline
		26.725	2.85		
		35.049	3.01		
2	Pr–PIn	11.776	5.28	29.59	Crystalline
		16.687	7.57		
		26.659	6.01		
		35.085	4.32		
		39.119	3.88		
3	Nd–PIn	09.399	2.37	57.86	Microcrystalline
		28.463	2.74		
		33.080	2.63		

against the applied temperature. The decomposition point obtained by the DSC curve is found between 661 and 681 °C showing its good stability against the heat. The absence of any endothermic peak at a lower temperature in the starting of the DSC curve indicates there is a lack of any moisture or volatile/water entity.

The TG-DTG curves indicates the weight loss of the oligomers in two steps: First, at a temperature of around 372 and 345 °C is due to degradation of the backbone chain of the polyindole skeleton [30,35,42,43]. The first weight loss found in PIn was around 372 °C showing the weight loss of 27.20% of the oligomer, whereas the catalyzed product i.e. La–PIn, Ce–PIn, Pr–PIn, and Nd–PIn showed the first decomposition at 341–349 °C with a weight loss of ~22%. The second weight loss was found in PIn at a somewhat lower temperature i.e. at 625 °C with ~34% weight loss leading the formation of a thermally stable heterodimer. The second weight loss of about 41% was found in La–PIn, Ce–PIn, Pr–PIn, and Nd–PIn at ~640 °C. After both weight losses, a dimer of indole which was interlinked by an oxygen atom was found stable. The 19.61% of the PIn sample was remained after annealing till 1400 °C, whereas the remaining percentage of the sample of La–PIn, Ce–PIn, Pr-PIn, and Nd–PIn are quite higher i.e. 21.29, 21.06, 20.40, 20.67%. These weight losses are summarized in Table 6. The results indicate that due to the presence of

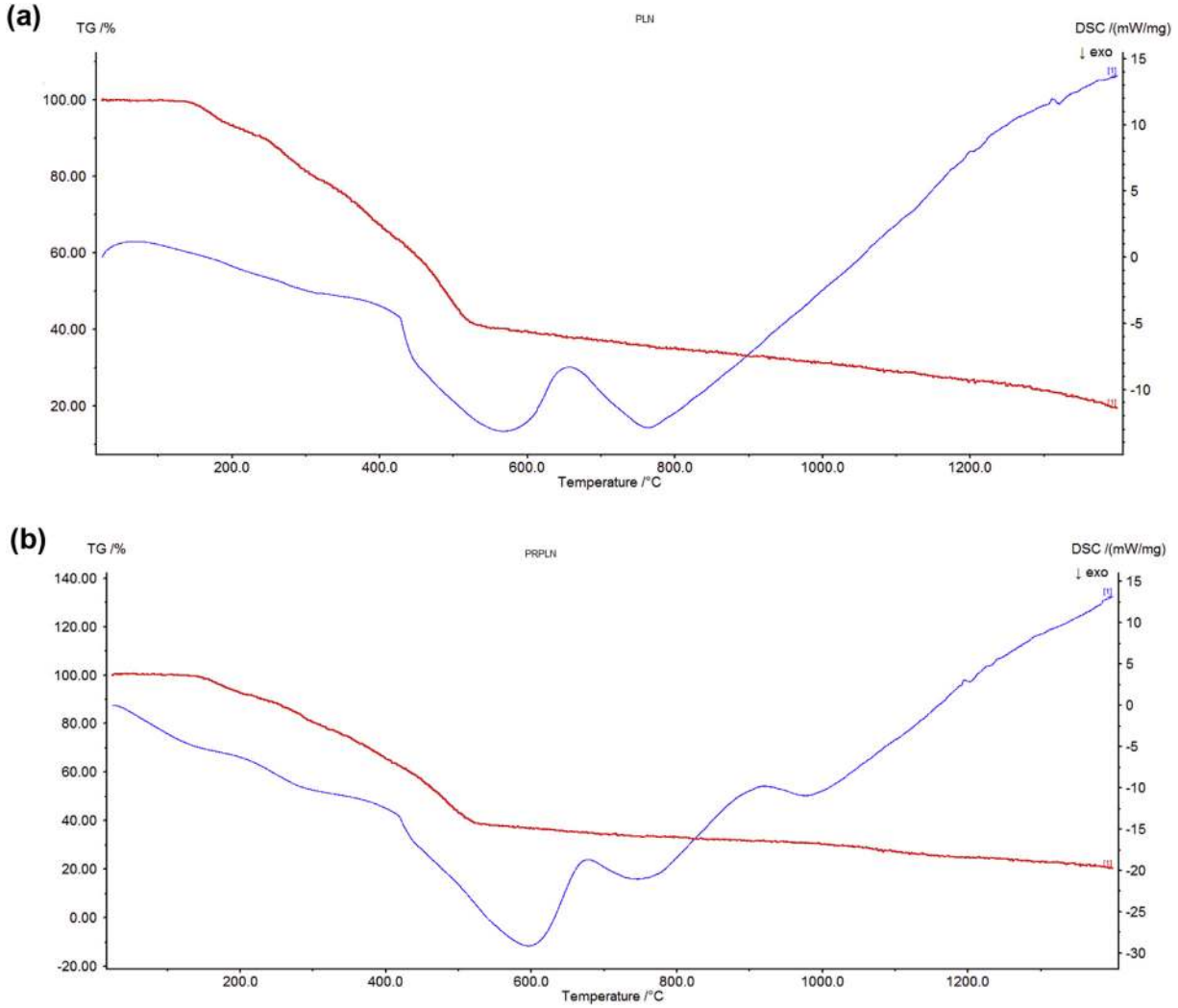

Fig. 3. (a)TG-DSC curves of PIn. (b)TG-DSC curves of La–PIn.

Table 6
Thermogravimetric decomposition pattern and stability towards temperature.

S. No.	Oligomer	M.P (°C)	Temperature (°C)	Weight loss %	Fragments lost	% Remain at 1400 °C
1	PIn	661	372	27.20	$C_{13}H_5N_1O_0$	19.61
			625	33.71	$C_{11}H_{10}N_2O_3$	
2	La–PIn	681	349	22.69	$C_{11}H_5N_1O_0$	21.29
			641	65.02	$C_{15}H_{10}N_2O_3$	
3	Ce–PIn	679	346	22.02	$C_{11}H_5N_1O_0$	21.06
			644	41.22	$C_{15}H_{10}N_2O_3$	
4	Pr–PIn	674	341	22.48	$C_{11}H_5N_1O_0$	20.40
			638	41.96	$C_{15}H_{10}N_2O_3$	
5	Nd–PIn	673	342	22.18	$C_{11}H_5N_1O_0$	20.67
			636	41.42	$C_{15}H_{10}N_2O_3$	

oxides of lanthanides they were decomposed at a higher temperature.

4.6. Study of magnetic behavior

The magnetic properties like magnetization (Ms), retentivity (Mr), coercivity (Hci) and effective magnetic moment (μ_{eff}) of oligomers have been studied by the M-H hysteresis curves. The hysteresis curve of one of the examples is given in Fig. 4. The nature of the curve indicates that the analyzed material could be slight paramagnetic. This statement is justified by the calculated value of effective magnetic moment which was obtained by the

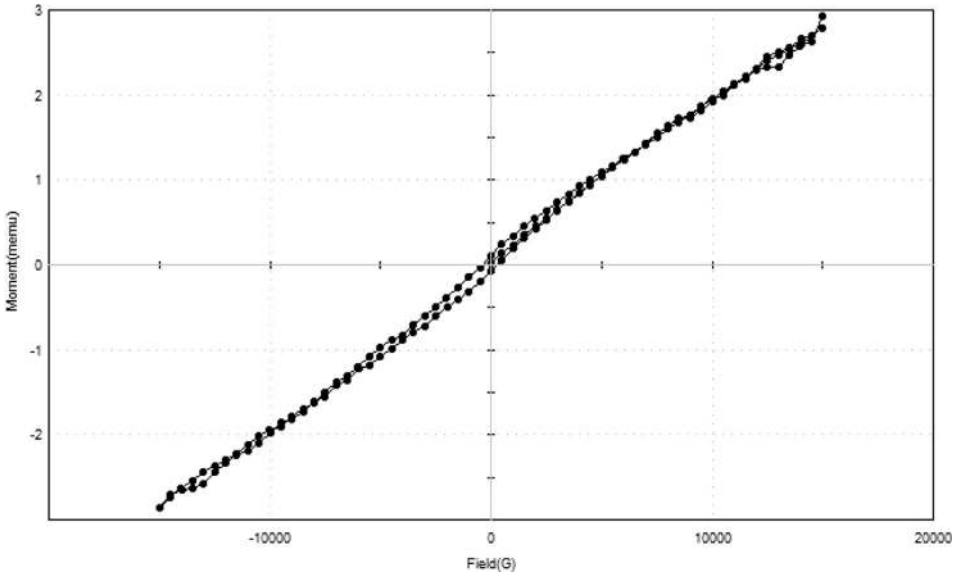

Fig. 4. M-H hysteresis loop of Pr–PIn showing paramagnetic nature of the oligomer.

magnetization, applied a magnetic field and molar susceptibility. The value of effective magnetic moment found to be above zero which sustains that these oligomers are paramagnetic. The magnetic properties including μ_{eff} of oligomers are given in Table 7.

4.7. Micrographic studies

To make known the particle sizes of differently synthesized and catalyzed oligomers of indole, they were subjected to SEM and TEM studies. From the SEM micrograph, the PIn, as well as all the catalyzed products (La–PIn, Ce–PIn, Pr–PIn, and Nd–PIn) were found to be of nanometer sized. From SEM studies it is depicted that all the differently synthesized hetero-oligomers have different morphology at its surface. The Pr–PIn and Ce–PIn have globular morphology, while the Nd–PIn has a fused structure at its surface. The La–PIn also shows globular morphology but tending to fuse with each other. Different morphology indicates the presence of different dopants in different materials. The sizes and shapes of these oligomers are given in Table 8 and these are seen in Fig. 5. The increase in the size of particles in comparison to the size of crystallite obtained by PXRD is due to the intermolecular hydrogen bonding which results in associated molecules of large particle size at the surface [44,45].

The inner core shell size of the particles/grain was obtained using TEM images. These particles/grains also have the size in nanometer range. By taking a particular example of Pr–PIn (Fig. 6) it can be seen that it has spindled shape structures which are overlapped with each other. The measured inner core shell size of this sample was found 0.19 nm (supplementary information SI 3a). The SAED patter reveals that this oligomer is of crystalline in nature (supplementary information SI 3b).

Table 7
Details of magnetic properties.

S. No.	Oligomer	Ms (emu)	Mr (emu)	Hci (G)	μ_{eff} (B.M)
1	PIn	2.96×10^{-3}	89.24×10^{-6}	325	0.011
2	La–PIn	2.90×10^{-3}	90.12×10^{-6}	326	0.014
3	Ce–PIn	2.84×10^{-3}	90.23×10^{-6}	326	0.016
4	Pr–PIn	2.89×10^{-3}	90.46×10^{-6}	327	0.031
5	Nd–PIn	2.80×10^{-3}	90.87×10^{-6}	327	0.024

Table 8
SEM microstructural investigation.

S. No.	Oligomer	Average particle size (nm)	Shape
1	PIn	232	Globular
2	La–PIn	315	Fused, irregular spheres
3	Ce–PIn	312	Globular
4	Pr–PIn	236	Globular
5	Nd–PIn	18	Fused

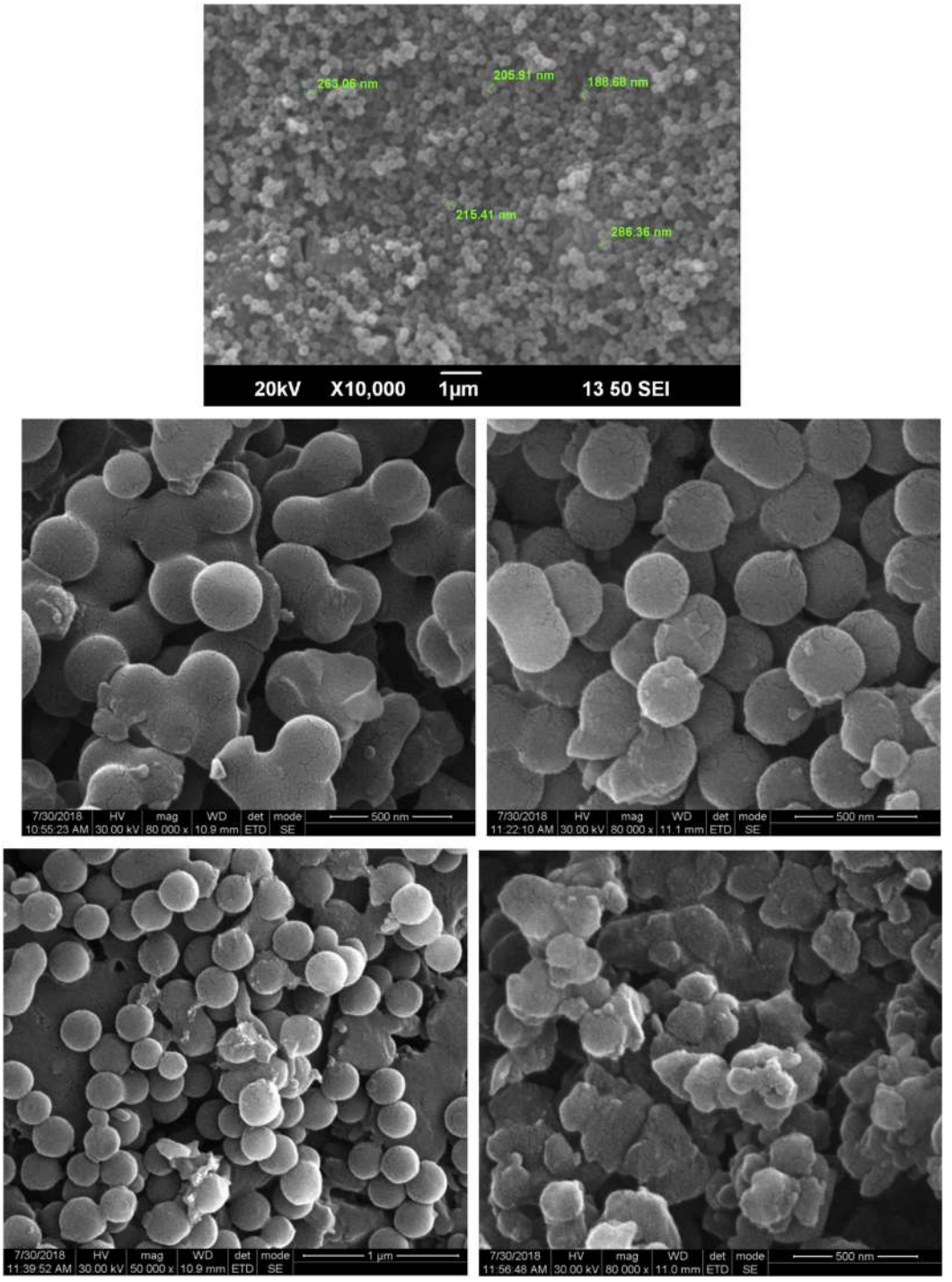

Fig. 5. SEM images of PIn, La–PIn, Ce–PIn, Pr–PIn and Nd–PIn.

4.8. Conductivity measurements

The conductivity of differently synthesized hetero-oligomers was studied in acetonitrile solution at room temperature. The reported value conductivity of acetonitrile is 7 $\mu\Omega^{-1}cm^{-1}$ and conductivity of indole was found around 58 $\mu\Omega^{-1}cm^{-1}$. The conductivity was measured at different

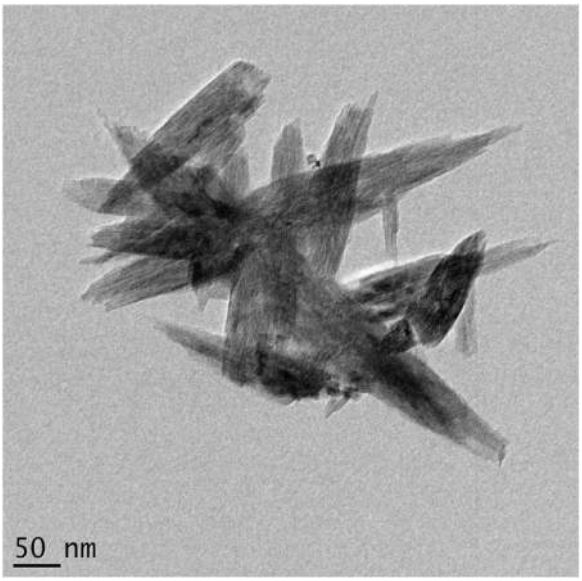

Fig. 6. TEM image of the oligomer Pr–PIn.

concentrations of indole as well as catalyzed and non-catalyzed hetero-oligomers. The hetero-oligomers showed high conductivity in comparison to its monomer, the reason can be the resonating structure formed by polymerization causes the polarity which leads to conductance. The indole showed very less effect of the change in concentration,

Table 9
Conductivity of different oligomers at various concentrations.

S. No.	Concentration (N)	Conductivity (S/cm) × 10^{-3}				
		PIn	*La–PIn*	*Ce–PIn*	*Pr–PIn*	*Nd–PIn*
1	0.04	50.9	52.3	52.0	55.6	59.9
2	0.02	82.1	83.5	85.7	85.9	84.8
3	0.0133	59.3	68.7	66.2	70.1	70.7
4	0.01	58.6	61.8	62.4	67.7	66.9

while the hetero-oligomers were showing a great variation with change in concentration. On increasing dilution, the ionization occurs easily hence conductance increases, whereas on further decreasing concentration, the ions per unit volume decrease leading to a decrease in conductance. The conductivity of these hetero-oligomers is found highest at N/50 concentration while decreasing or increasing concentration the conductivity decreases steeply. The conductivity dependence of concentration is clearly shown in Fig. 7 and the related details are summarized in Table 9. The conductivity is in the range of 10^{-3} S cm^{-1}, which is close to the literature value [41] which tells that the polymerized indole using $FeCl_3$ oxidant follows the same order. Their conductivity study shows that these oligomers can be used as a semiconductor. This statement is supported by the tauc-plot of oligomers [supplementary information SI 4]

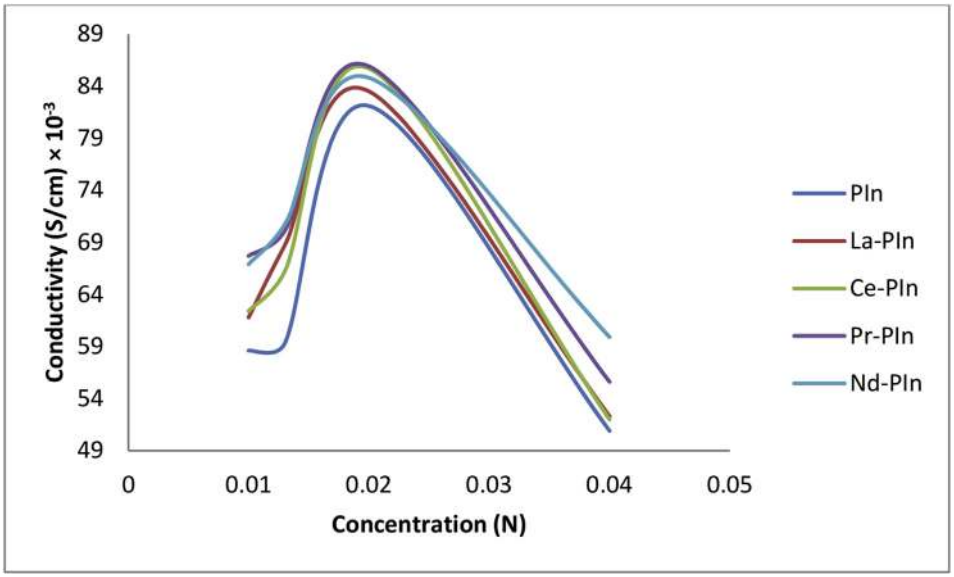

Fig. 7. Conductive measurement of different oligomers with respect to concentration.

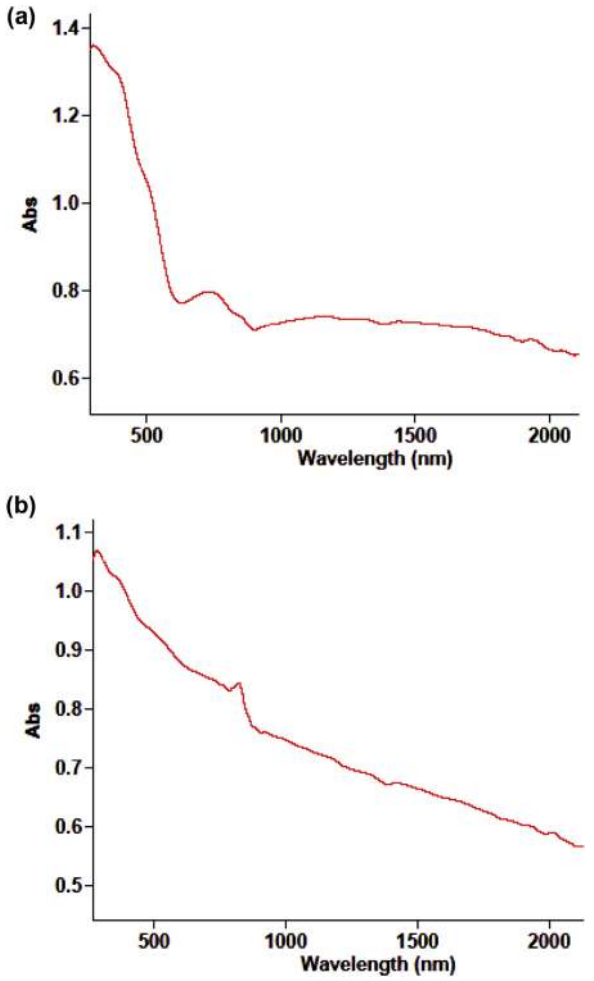

Fig. 8. (a)Absorption spectrum of PIn.(b)Absorption spectrum of La–PIn.

showing the bandgap which resembles the property of a semiconductor.

4.9. Absorption, excitation and emission studies

The non-catalyzed hetero oligomer shows an absorption peak at around 722 nm, whereas the catalyzed hetero-oligomers exhibit absorption in the range 808–824 nm. All these peaks resemble the existence of polaron in the indole oligomers [46–48]. The electric conductivity is somewhat due to the presence of this polaron [47]. These peaks are given in Fig. 8.

To study the luminescence behavior of the indole oligomers, excitation and emission studies have been done. The absorption, emission and excitation maxima of different types of oligomers are given in Table 10. From the given Table 10 it can be seen that the emission maxima are found at a somewhat lower wavelength concerning its excitation maxima. This is due to the triplet-triplet annihilation and Dexter-type energy transfer. This phenomenon is known as the upconversion of the photon. This leads to the upconversion of violet light to the far IR region. The Dexter type energy transfer is nonlinear energy transfer which involves multiple steps [49,50]. The triplet-triplet annihilation system consists of a sensitizer which acts as a donor and another species which act as acceptor or Annihilator. The donor should have a narrow singlet-triplet gap which upon absorption of photon allows forming excitation of triplet state via intersystem crossing, which further transfers energy to the chromophore [51–55]. The chromophore should have a large singlet-triplet gap and forbidden intersystem crossing and should also have high quantum yield [56–61].

Table 10
Details of luminescence properties the oligomers.

S. No.	Oligomer	Absorption maxima (nm)	Excitation maxima (nm)	Emission maxima (nm)	Anti-stoke Shift
1	PIn	722	427	395	32
2	La–PIn	824	429	395	34
3	Ce–PIn	808	430	395	35
4	Pr–PIn	812	429	394	35
5	Nd–PIn	819	428	395	33

In the case of synthesized oligomers, the indole moiety with an oxygen atom (having a narrow singlet-triplet gap due to the presence of oxygen) acts as an anti-aromatic photosensitizer and the indole moiety solely act as acceptor (having a large singlet-triplet gap and high quantum yield). On absorbing energy C_8H_5NO (which originally has 10π electron systems) loses its aromaticity due to the presence of oxygen and produces metastable Baird anti-aromatic triplet species. This sensitizer transfers its energy to acceptor via intersystem crossing and regeneration of ground state sensitizer occurs. This process is repeated to form another long-lived excited triplet acceptor. The interaction of two triplet excited acceptors via secondary energy transfer process leads to the triplet-triplet annihilation. In triplet-triplet annihilation, the triplet

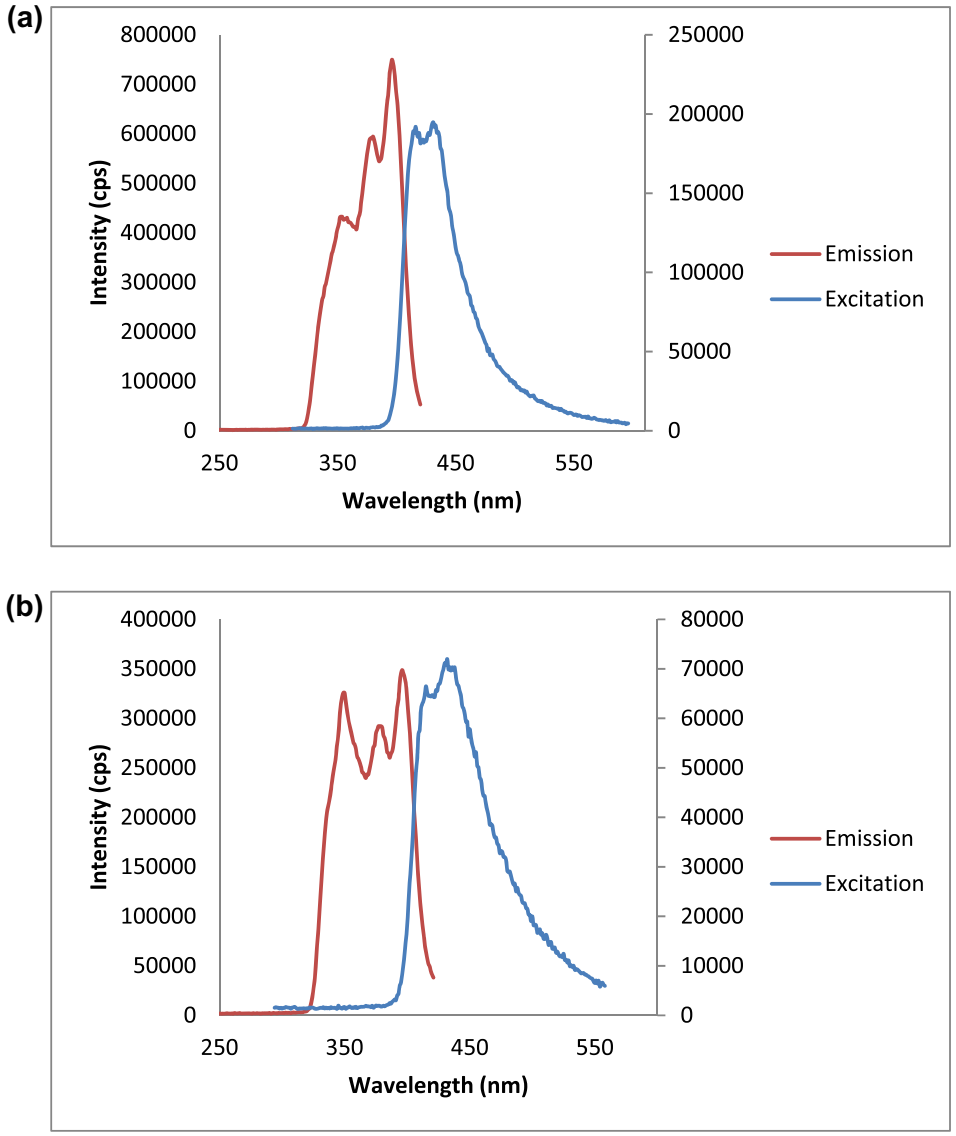

Fig. 9. (a)Excitation and emission spectrum of PIn. (b)Excitation and emission spectrum of La–PIn.

energies combine which converts low energy photons to high energy photons [53,62,63]. High energy photon results in low wavelength which is clearly seen in Fig. 9.

5. Conclusions

The indole monomers were polymerized effectively with the help of different $LnCl_3$. In contrast to previous reports, the temperature was elevated to increase the collision of the molecules which leads to the decrease the reaction time. The FTIR and NMR studies reveal that the polymerization occurs from the 2nd and 3rd position of the five-membered ring of indole, leaving the –NH position as such. The mass spectrometry confirms the existence of polyindole as a pentamer. TG studies indicate the thermal behavior and stability of the oligomer with respect to temperature. The conductivity measurement depicted that these oligomers show the electrical conductivity comparable to previously synthesized polyindoles. The absorption spectrum indicates the existence of polaron in the oligomer structure. The value of emission maxima shows that there is a phenomenon of photon upconversion occurs.

The $LnCl_3$ was used to tune the shape and sizes of indole oligomers, to decrease the reaction time and to enhance the semiconducting properties as well. Since these lanthanide elements are positively charged carriers hence these materials can act as a p-type semiconductor. In the future, we will explore the effect of the addition of all lanthanide salts on the sizes and shapes of indole oligomers.

Funding

This research work is not supported by any funding agency.

Declaration of Competing Interest

None.

Abbreviations

PIn Non-catalyzed indole oligomer; In–O–In (Undoped)
La–PIn In–O–In catalyzed and doped by $LaCl_3 \cdot 7H_2O$ (Dopant: Lanthanum)
Ce–PIn In–O–In catalyzed and doped by $CeCl_3 \cdot 7H_2O$ (Dopant: Cerium)
Pr–PIn In–O–In catalyzed and doped by $PrCl_3 \cdot 6H_2O$ (Dopant: Praseodymium)
Nd–PIn In–O–In catalyzed and doped by $NdCl_3 \cdot 6H_2O$ (Dopant: Neodymium)

References

[1] A. Turut, F. Koleli, Metallic polythiophene/inorganic semiconductor Schottky diodes, Phys. B 192 (1993) 279–283, https://doi.org/10.1016/0921-4526(93)90032-2.
[2] J. Heinze, Electrochemistry of conducting polymers, Synth. Met. 43 (1991) 2805–2823, https://doi.org/10.1016/0379-6779(91)91183-B.
[3] S.H. Hosseini, S.H.A. Oskooe, A.A. Entezami, Toxic gas and vapour detection with polyaniline gas sensors, Iran. Polym. J. (Engl. Ed.) 14 (2005) 333–343. http://citeseerx.ist.psu.edu/viewdoc/download?doi=10.1.1.558.3502&rep=rep1&type=pdf.
[4] G. Sivaprasad, P.T. Perumal, V.R. Prabavathy, N. Mathivanan, Synthesis and anti-microbial activity of pyrazolylbisindoles–promising anti-fungal compounds, Bioorg. Med. Chem. Lett 16 (2006) 6302–6305, https://doi.org/10.1016/j.bmcl.2006.09.019.
[5] M.R. Nabid, R. Sedghi, A. Bagheri, M. Behbahani, M. Taghizadeh, H.A. Oskooie, M.M. Heravi, Preparation and application of poly(2-amino thiophenol)/MWCNTs nanocomposite for adsorption and separation of cadmium and lead ions via solid phase extraction, J. Hazard Mater. 203–204 (2012) 93–100, https://doi.org/10.1016/j.jhazmat.2011.11.096.
[6] M.R. Nabid, R. Sedghi, M. Behbahani, B. Arvan, M.M. Heravi, H.A. Oskooie, Application of Poly 1,8 diaminonaphthalene/multiwalled carbon nanotubes-COOH hybrid material as an efficient sorbent for trace determination of cadmium and lead ions in water samples, J. Mol. Recogn. 27 (2014) 421–428, https://doi.org/10.1002/jmr.2361.
[7] E.G. Kalhor, M. Behbahani, J. Abolhasani, R.H. Khanmiri, Synthesis and characterization of modified multiwall carbon nanotubes with poly (N-phenylethanolamine) and their application for removal and trace detection of lead ions in food and environmental samples, Food Anal. Methods 8 (2015) 1326–1334, https://doi.org/10.1007/s12161-014-0001-x.
[8] M. Behbahani, A. Bagheri, T. Gorji, M.R. Nabid, R. Sedghi, H.A. Oskooie, M.M. Heravi, Application of Poly (N-Phenylethanolamine) Modified MWCNTs as a New Sorbent for Solid-phase Extraction of Trace Palladium Ions in Soil and Water Samples, Sample Preparation, 2013, pp. 10–17, https://doi.org/10.2478/sampre-2013-0002.
[9] R. Sedghi, M.R. Nabid, M. Shariati, M. Behbahani, H.R. Moazzami, Preparation of PAN-based electrospun nanofiber webs containing Ni-ZnO as high performance visible light photocatalyst, Fibers Polym. 17 (2016) 1969–1976, https://doi.org/10.1007/s12221-016-6731-1.
[10] G. Tourillon, F. Gamier, New electrochemically generated organic conducting polymers, J. Electroanal. Chem. 135 (1982) 173–178, https://doi.org/10.1016/0022-0728(82)90015-8.
[11] K. Phasuksom, A. Sirivat, Synthesis of nano-sized polyindole via emulsion polymerization and doping, Synth. Met. 219 (2016) 142–153, https://doi.org/10.1016/j.synthmet.2016.05.033.
[12] D. Billaud, E.B. Maarouf, E. Hannecart, An investigation of electrochemically and chemically polymerized indole, Mater. Res. Bull. 29 (1994) 1239–1246, https://doi.org/10.1016/0025-5408(94)90147-3.
[13] S.P. Koiry, V. Saxena, D. Sutar, S. Bhattacharya, D.K. Aswal, S.K. Gupta, J.V. Yakhmi, Interfacial synthesis of long polyindole fibers, J. Appl. Polym. Sci. 103 (2007) 595–599, https://doi.org/10.1002/app.25245.
[14] A. Shuying, T. Abdiryim, Y. Ding, I. Nurulla, A comparative study of the microemulsion and interfacial polymerization for polyindole, Mater. Lett. 62 (2008) 935–938, https://doi.org/10.1016/j.matlet.2007.07.014.
[15] F. Caruso, R.A. Caruso, H. Mahowald, Nanoengineering of inorganic and hybrid hollow spheres by colloidal templating, Science 282 (1998) 1111–1114, https://doi.org/10.1126/science.282.5391.1111.
[16] Y. Xia, B. Gates, Y. Yin, Y. Lu, Monodispersed colloidal spheres:old materials with new applications, Adv. Mater. 12 (2000) 693–713, https://doi.org/10.1002/(SICI)1521-4095(200005)12:10<693::AID-ADMA693>3.0.CO;2-J.
[17] R. Gref, Y. Minamitake, M.T. Peracchia, V. Torchilin, R. Langer, Biodegradable long-circulating polymeric nanospheres, Science 263 (1994) 1600–1603, https://doi.org/10.1126/science.8128245.
[18] D. Zhao, J. Fang, Q. Huo, N. Meloch, G.H. Fredriction, B.F. Chmelka, G.D. Strucky, Triblock copolymer syntheses of mesoporous silica with periodic 50 to 300 angstrom pores,

Science 279 (1998) 548−552, https://doi.org/10.1126/science.279.5350.548.
[19] N. Nuraje, K. Su, N.I. Yang, H. Matsui, Liquid/Liquid interfacial polymerization to grow single crystalline nanoneedles of various conducting polymers, ACS Nano 2 (2008) 502−506, https://doi.org/10.1021/nn7001536.
[20] W. Li, M. Zhu, Q. Zhang, D. Chen, Expanded conformation of macromolecular chain in polyaniline with one-dimensional nanostructure prepared by interfacial polymerization, Appl. Phys. Lett. 89 (2006) 103110−103113, https://doi.org/10.1063/1.2345376.
[21] J. Huang, S. Virji, B.H. Weiller, R.B. Kaner, Nanofiber formation in the chemical polymerization of aniline, J. Am. Chem. Soc. 126 (2004) 851−855, https://doi.org/10.1021/ja0371754.
[22] G. Rajasudha, D. Rajeswari, B. Lavanya, R. Saraswathi, S. Annapoorni, N.C. Mehra, Colloidal dispersions of polyindole, Colloid Polym. Sci. 283 (2005) 575−582, https://doi.org/10.1007/s00396-004-1189-x.
[23] G.F. Smith, The dimerization and trimerization of indole, Chem. Ind. (1954) 1451−1452. https://ci.nii.ac.jp/naid/10013143498/.
[24] V. Bocchi, G. Palla, Synthesis and characterization of new indole trimers and tetramers, Tetrahedron 42 (1986) 5019−5024, https://doi.org/10.1016/S0040-4020(01)88053-4.
[25] K.M. Ziadan, New Polymer for Special Applications, Intech Open, UK, 2012, https://doi.org/10.5772/48316.
[26] D. Billaud, B. Humbert, L. Thevenot, P. Thomas, H. Talbi, Electrochemical properties and fourier transform-infrared spectroscopic investigations of the redox behaviour of poly(-indole-5-carboxylic acid) in $LiClO_4$_Acetonitrile solutions, Spectrochim. Acta, Part A 59 (2003) 163−168, https://doi.org/10.1016/S1386-1425(02)00150-6.
[27] K.S. Ryu, N.G. Park, K.M. Kim, Y.G. Lee, Y.J. Park, S.J. Lee, C.K. Jeong, J. Joo, S.H. Chang, The physicochemical properties of polyindole/thiol composites, Synth. Met. 135−136 (2003) 397−398, https://doi.org/10.1016/S0379-6779(02)00648-3.
[28] S.L. Mu, Electrochemical copolymerization of aniline and o-aminophenol, Synth. Met. 143 (2004) 259−268, https://doi.org/10.1016/j.synthmet.2003.12.008.
[29] H. Talbi, J. Ghanbaja, D. Billaud, B. Humbert, Vibrational properties and structural studies of doped and dedoped polyindole by FTIR, Raman and EEL spectroscopies, Polymer 38 (1997) 2099−2106, https://doi.org/10.1016/S0032-3861(96)00759-8.
[30] C. Zhijiang, Y. Guang, Synthesis of polyindole and its evaluation for Li-ion battery applications, Syn. Met 160 (2010) 1902−1905, https://doi.org/10.1016/j.synthmet.2010.07.007.
[31] S. Mohan, N. Sundaraganesan, FTIR and Raman studies on bemimidamle, Spectrochim. Acta, Part A 47 (1991) 1111−1115, https://doi.org/10.1016/0584-8539(91)80042-H.
[32] M. Garg, J.K. Quamara, FTIR analysis of high energy heavy ion irradiated kapton-H polyimide, Int. J. Pure Chem. 45 (2007) 563−568. http://nopr.niscair.res.in/handle/123456789/2630.
[33] T. Kondo, C. Sawatari, R.S.J. Manley, D.G. Gray, Characterization of hydrogen bonding in cellulose-synthetic polymer blend systems with regioselectively substituted methylcellulose, Macromolecules 27 (1994) 210−215, https://doi.org/10.1021/ma00079a031.
[34] M. Yurtsever, E. Yurtsever, A DFT study of polymerization mechanisms of indole, Polymer 43 (2002) 6019−6025, https://doi.org/10.1016/S0032-3861(02)00510-4.
[35] N.B. Taylan, B. Sari, H.I. Unal, Preparation of conducting poly(vinyl chloride)/polyindole composites and freestanding films via chemical polymerization, J. Polym. Sci. Part B 48 (2010) 1290−1298, https://doi.org/10.1002/polb.22023.
[36] B. Coban, U. Yildiz, A. Sengul, Synthesis, characterization, and DNA binding of complexes [Pt(bpy)(pip)]2+ and [Pt(bpy)(hpip)]2+, J. Biol. Inorg. Chem. 18 (2013) 461−471, https://doi.org/10.1007/s00775-015-1317-8.
[37] I. Ameen, A.K. Tripathi, A. Siddiqui, G. Kapil, S.S. Pandey, U.N. Tripathi, Synthesis, characterizations and photo-physical properties of novel lanthanum(III) complexes, J. Taibah Univ. Med. Sci. 12 (2018) 796−808, https://doi.org/10.1080/16583655.2018.1516028.
[38] H. Talbi, E.B. Maarouf, B. Humbert, M. Alnot, J.J. Ehrhardt, J. Ghanbaja, D. Billaud, Spectroscopic studies of electrochemically doped polyindole, J. Phys. Chem. Solid. 57 (1996) 1145−1151, https://doi.org/10.1016/0022-3697(95)00413-0.
[39] Q.B. Zhang, C. Yang, Y.X. Hua, Y. Li, P. Dong, Electrochemical preparation of nanostructured lanthanum using lanthanum chloride as a precursor in 1-butyl-3-methylimidazolium dicyanamide ionic liquid, Phys. Chem. Chem. Phys. 17 (2015) 4701−4707, https://doi.org/10.1039/C4CP05266H.
[40] K. Cheraitia, A. Lounis, M. Mehenni, M. Azzaz, K. Osmane, Neutron activation analysis of Nd-Fe-B magnet and determination of the content of Nd after oxalate precipitation and production of Nd_2O_3, Matter: Int. J. Sci. Technol. 1 (2015) 259−274, https://doi.org/10.20319/mijst.2016.s11.259274.
[41] A. Abbasalizadeh, L. Teng, S. Sridhar, S. Seetharaman, Neodymium extraction using salt extraction process, Miner. Process. Extr. Metall. Trans. Inst. Min. Metall. C 124 (2015) 191−198, https://doi.org/10.1179/1743285514Y.0000000062.
[42] N.S. Asik, R. Tas, S. Sonmezoglu, M. Can, G. Cankaya, Monomer effect on stability, electrical conductivity and combination of aniline−indole copolymer synthesized with H_5IO_6, J. Non-Cryst. Solids 356 (2010) 1848−1853, https://doi.org/10.1016/j.jnoncrysol.2010.06.020.
[43] P.S. Abthagir, R. Saraswathi, Charge transport and thermal properties of polyindole, polycarbazole and their derivatives, Thermochim. Acta 424 (2004) 25−35, https://doi.org/10.1016/j.tca.2004.04.028.
[44] I. Ameen, A.K. Tripathi, R.L. Mishra, A. Siddiqui, U.N. Tripathi, Luminescent, optical, magnetic and meta-material behavior of cerium complexes, J. Saudi Chem. Soc. 23 (2019) 725−739, https://doi.org/10.1016/j.jscs.2018.12.003.
[45] I. Ameen, A.K. Tripathi, R.L. Mishra, A. Siddiqui, U.N. Tripathi, Aging effect on bonding properties of fluorescent neodymium materials, Karbala Int. J. Mod. Sci. 4 (2018) 258−273, https://doi.org/10.1016/j.kijoms.2018.05.001.
[46] C.R.K. Rao, R. Muthukannan, M. Vijayan, Studies on biphenyl disulphonic acid doped polyanilines: synthesis, characterization and electrochemistry, Bull. Mater. Sci. 35 (2012) 405−414, https://doi.org/10.1007/s12034-012-0315-5.
[47] S. Jayasudha, L. Priya, K.T. Vasudevan, Structural, optical and electricalcharacterization of polyaniline/silver nanocomposites, Int. J. Res. Eng. Technol. 5 (2016) 303−307. https://ijret.org/volumes/2016v05/i16/IJRET20160516067.pdf.

[48] A. Balkan, E. Armagan, G. Ozaydin, I. Beilstein, Synthesis of coaxial nanotubes of polyaniline and poly(hydroxyethyl methacrylate) by oxidative/initiated chemical vapor deposition, J. Nanotechnol. 8 (2017) 872−882. https://www.beilstein-journals.org/bjnano/articles/8/89.

[49] M.K. Manna, S. Shokri, G.P. Wiederrecht, D.J. Gosztola, A.J.L. Ayitou, New perspectives for triplet−triplet annihilation based photon upconversion using all-organic energy donor & acceptor chromophores, Chem. Commun. 54 (2018) 5809−5818, https://doi.org/10.1039/C8CC01553H.

[50] T.N.S. Rachford, F.N. Castellano, Photon upconversion based on sensitized triplet−triplet annihilation, Coord. Chem. Rev. 254 (2010) 2560−2573, https://doi.org/10.1016/j.ccr.2010.01.003.

[51] J. Jayabharathi, V. Thanikachalam, K. Jayamoorthy, Antioxidant benzimidazole bind bovine serum albumin, J. Photochem. Photobiol., B 115 (2012) 85−92, https://doi.org/10.1016/j.jphotobiol.2012.06.014.

[52] C. Karunakaran, J. Jayabharathi, K. Jayamoorthy, Photoinduced electron transfer from benzimidazole to nano WO_3, CuO and Fe_2O_3. A new approach on LUMO−CB energy-binding efficiency relationship Sensors, Actuators B 182 (2013) 514−520, https://doi.org/10.1016/j.snb.2013.03.051.

[53] C. Karunakaran, J. Jayabharathi, R. Sathishkumar, K. Jayamoorthy, Interaction of fluorescent sensor with superparamagnetic iron oxide nanoparticles, Spectrochim. Acta, Part A 110 (2013) 151−156, https://doi.org/10.1016/j.saa.2013.03.042.

[54] P. Saravanan, K. Jayamoorthy, S. Anandakumar, Switch-On fluorescence and Photo-induced electron transfer of 3-aminopropyltriethoxysilane to ZnO: dual applications in sensors and antibacterial activity, Sensor. Actuator. B 221 (2015) 784−791, https://doi.org/10.1016/j.snb.2015.05.069.

[55] S. Suresh, K. Jayamoorthy, S. Karthikeyan, Fluorescence sensing of potential NLO material by bunsenite NiO nanoflakes: room temperature magnetic studies, Sensor. Actuator. B 232 (2016) 269−275, https://doi.org/10.1016/j.snb.2016.03.149.

[56] A. Monguzzi, R. Tubino, S. Hoseinkhani, M. Campione, F. Meinardi, Low power, non-coherent sensitized photon upconversion: modelling and perspectives, Phys. Chem. Chem. Phys. 14 (2012) 4322−4332, https://doi.org/10.1039/C2CP23900K.

[57] T.F. Schulze, T.W. Schmidt, Photochemical upconversion: present status and prospects for its application to solar energy conversion, Energy Environ. Sci. 8 (2015) 103−125, https://doi.org/10.1039/C4EE02481H.

[58] C. Karunakaran, J. Jayabharathi, K. Jayamoorthy, Fluorescence enhancing and quenching of TiO_2 by benzimidazole, Sensor. Actuator. B 188 (2013) 207−211, https://doi.org/10.1016/j.snb.2013.07.008.

[59] S. Suresh, K. Jayamoorthy, P. Saravanan, S. Karthikeyan, Switch-Off fluorescence of 5-amino-2-mercapto benzimidazole with Ag_3O_4nanoparticles: experimental and theoretical investigations, Sensor. Actuator. B 225 (2016) 463−468, https://doi.org/10.1016/j.snb.2015.11.056.

[60] V. Gray, V. Dzebo, M. Abrahamsson, B. Albinsson, K. Moth-Poulsen, Triplet-triplet annihilation photon-upconversion: towards solar energy applications, Phys. Chem. Chem. Phys. 16 (2014) 10345−10352, https://doi.org/10.1039/C4CP00744A.

[61] N.J. Turro, V. Ramamurthy, J.C. Scaiano, Modern Molecular Photochemistry of Organic Molecules, University Science Books, 2010.

[62] C. Karunakaran, J. Jayabharathi, K.B. Devi, K. Jayamoorthy, Photosensitization of imidazole derivative by ZnO nanoparticle, J. Fluoresc. 22 (2012) 1047−1053, https://doi.org/10.1007/s10895-012-1042-4.

[63] C. Karunakaran, J. Jayabharathi, V. Kalaiarasi, K. Jayamoorthy, Enhancing photoluminescent behavior of 2-(naphthalen-1-yl)-1,4,5-triphenyl-1H-imidazole by ZnO and Bi_2O_3, Spectrochim. Acta, Part A 118 (2014) 182−186, https://doi.org/10.1016/j.saa.2013.08.098.